



# Tofu-derived carbon framework with embedded ultrasmall tin nanocrystals for high-performance energy storage devices



Geon-Hyoung An <sup>a</sup>, Do-Young Lee <sup>b</sup>, **Hyo-Jin Ahn** <sup>a, b, \*</sup>

<sup>a</sup> Program of Materials Science & Engineering, Convergence Institute of Biomedical Engineering and Biomaterials, Seoul National University of Science and Technology, Seoul 139-743, South Korea

<sup>b</sup> Department of Materials Science and Engineering, Seoul National University of Science and Technology, Seoul 139-743, South Korea

## ARTICLE INFO

### Article history:

Received 9 March 2017

Received in revised form

2 June 2017

Accepted 5 June 2017

Available online 8 June 2017

### Keywords:

Li-ion batteries

Recycling

Food waste

Spoilt tofu

Ultrasmall Sn nanocrystals

Porous carbon framework

## ABSTRACT

Carbon materials as intra-electrode frameworks for energy storage devices have received noticeable attention due to their high porosity, high electrical conductivity, and excellent chemical and physical stability. Nevertheless, the utilisation of these frameworks still faces significant challenges such as limited raw material resources, complicated synthetic process, high-temperature synthesis, and high production costs. Herein, we report a unique and facile approach to synthesise a spoilt tofu-derived carbon framework with embedded ultrasmall Sn nanocrystals (SCS) derived from food waste (such as spoilt tofu) using simple impregnation and carbonisation. The unique architecture of SCS was due to the porous structure of spoilt tofu and was utilised as an anode for Li-ion batteries. The optimised SCS architecture shows excellent electrochemical performance with outstanding cycling stability (621 mA h g<sup>-1</sup> capacity retention up to 100 cycles) and excellent high-rate performance (250 mA h g<sup>-1</sup> at 2000 mA g<sup>-1</sup>). Thus, this facile approach provides helpful synergistic effects in terms of structural stability, electrochemical active surface area, and shorter diffusion pathways for Li ions. Consequently, the recycling strategy of spoilt tofu food waste could provide a unique route to low-cost production of high-performance Li-ion batteries.

© 2017 Elsevier B.V. All rights reserved.

## 1. Introduction

Owing to the growing global population, the increasing quantities of food waste in our society have resulted in severe environmental pollution [1,2]. Accordingly, the United States Environmental Protection Agency suggested a 50% reduction of food waste by the year 2030 to protect the world from climate change and conserve natural resources [3]. Currently, the standard procedure for removing food waste is burying it underground, which itself causes secondary environmental pollution, as shown in Fig. 1a [2]. As a result, sustainable food waste recycling (Fig. 1b) is essential to economically improve the environment and save fuel.

Among the different types of food waste, spoilt tofu has been used as a raw carbon source for the synthesis of multifunctional carbon materials due to its high porosity (~85%). Tofu consists of water, protein, and fat, and is derived from soybeans, which are

becoming increasingly popular worldwide due to being cholesterol-free and rich in nutrients such as vitamins, minerals, omega-3 fatty acids, and isoflavone [4,5]. However, tofu that is past its due date is sent back to the factory and disposed [4,5]. Thus, the recycling of spoilt tofu is essential for both financial and environmental reasons. The spoilt tofu can be easily transformed into macroscale carbon materials widely used in various electronic applications [4,5]. It is well known that carbon materials with high porosity, high electrical conductivity, and chemical and physical stability have received considerable attention due to their promising applications in fields such as Li-ion batteries (LIBs), supercapacitors, fuel cells, and absorbents [6–8]. However, the optimised utilisation of spoilt tofu food waste for fabricating multifunctional carbon materials by chemical impregnation has not yet been studied. Among the promising applications of carbon materials derived from spoilt tofu, LIBs have drawn extensive attention due to their excellent characteristics, such as high energy density, excellent cycling stability, environmental friendliness, absence of memory effect, and low self-discharge rate [9,10]. However, to advance LIB technology in the direction of pragmatic applications, further development of LIB anodes is essential to meet the

\* Corresponding author. Department of Materials Science and Engineering, Seoul National University of Science and Technology, Seoul 139-743, South Korea.

E-mail address: [hjahn@seoultech.ac.kr](mailto:hjahn@seoultech.ac.kr) (H.-J. Ahn).

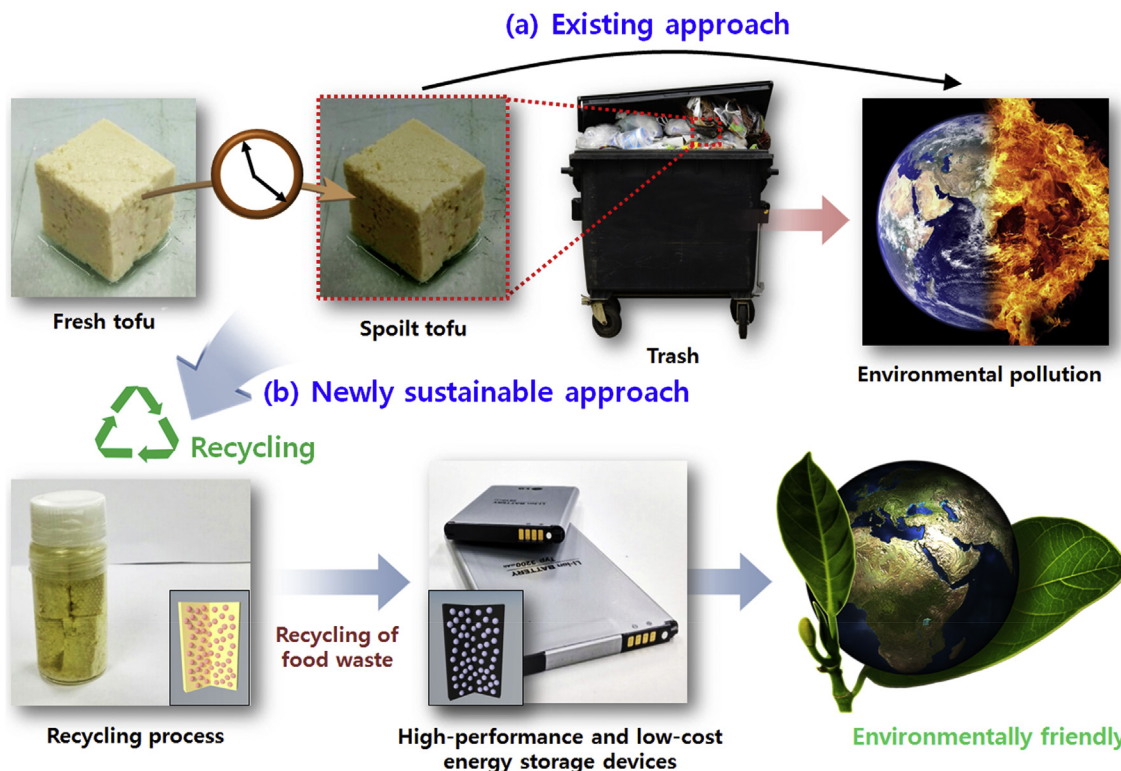


**Fig. 1.** Schematics of the newly sustainable approach using the recycling of food waste. (a) Standard procedure for removing food waste resulting in secondary environmental pollution. (b) Recycling of food waste using a sustainable approach with eco-friendly materials.

industrial requirements; as a key component, the anode plays a major role in determining cost effectiveness, performance, weight, and volume [11,12]. Currently, commercial LIB technology generally employs synthetic graphite due to its stable cycling performance. However, critical problems such as limited raw material resources, complicated synthetic process, and high-temperature synthesis is still unresolved, leading to high synthetic graphite production costs. Thus, the recycling of spoiled tofu raw materials using a simple strategy could be an effective solution for LIB price reduction. In addition, another issue of carbon materials is their low theoretical specific capacity of  $372 \text{ mA h g}^{-1}$ , leading to poor energy storage performance [13]. Therefore, to improve the specific capacity, metal-based materials with high theoretical capacity should be used. However, the latter always suffer from rapid capacity fading arising from structural degradation and electrical contact loss during cycling.

To overcome these problems, framework carbon materials are efficiently employed, thus, preventing the severe volume expansion stress of metal-based materials [14–16]. Nevertheless, higher capacity and better cycling stability are still required for practical applications of LIBs, such as electric vehicles and hybrid electric vehicles. Thus, these approaches need innovative schemes to control the ultrasmall size ( $\sim 2 \text{ nm}$ ) and excellent dispersion of metal nanocrystals that are required to increase the number of electro-active sites in the advanced carbon framework derived from spoiled tofu. Therefore, the development of a unique and facile approach to effectively obtain ultrasmall metal nanocrystals and carbon framework composites as well as to reduce the cost is critical for high-performance and low-cost LIBs, which has not yet been studied.

Herein, we report the unique architecture of a spoiled tofu-derived carbon framework with embedded ultrasmall Sn nanocrystals (SCS) containing a typical high-capacity metal (Sn:  $992 \text{ mA h g}^{-1}$ ) synthesised from recycled carbon materials (spoilt

tofu) using simple impregnation and carbonisation [17–19].

## 2. Experimental section

### 2.1. Materials

Tofu was purchased from (Pulmuone Co., Ltd., Korea). To obtain the spoiled tofu, we had left the fresh Tofu for one week after the expiration date at  $5^\circ \text{C}$ . Tin(II) chloride dihydrate ( $\text{SnCl}_2 \cdot 2\text{H}_2\text{O}$ ) were purchased from Sigma-Aldrich used without further purification.

### 2.2. Synthesis of spoiled tofu-derived carbon framework with embedded ultrasmall Sn nanocrystals (SCS)

First,  $\text{SnCl}_2 \cdot 2\text{H}_2\text{O}$  was dissolved in 10 mL ethanol under vigorous stirring for 1 h. The spoiled tofu was cut by a knife in a size of  $1 \text{ cm}^3$  and then impregnated with prepared solution for 12 h. After impregnation, the solution was extracted and then dried in an oven at  $80^\circ \text{C}$ . The impregnated spoiled tofu was stabilized at  $300^\circ \text{C}$  for 2 h in air and broken by ball milling for one week. Finally, the stabilized tofu was carbonized at  $800^\circ \text{C}$  for 2 h in nitrogen atmosphere to obtain a SCS. Finally, the prepared SCS was broken by ball milling.

Also, the four types of composites prepared using 20, 30, and 40 wt%  $\text{SnCl}_2 \cdot 2\text{H}_2\text{O}$  are hereafter referred to as SCS-20, SCS-30, and SCS-40, respectively. For comparison, the carbon framework using only spoiled tofu without  $\text{SnCl}_2 \cdot 2\text{H}_2\text{O}$  were prepared using the above-mentioned method.

### 2.3. Characterization

The structures and morphologies were investigated examined by scanning electron microscopy (SEM, Hitachi S-4800) and transmission electron microscopy (TEM, MULTI/TEM; Tecnai G<sup>2</sup>,

KBSI Gwangju Center). A Phillips CM20T/STEM equipped with energy-dispersive X-ray spectrometry (EDS) was used for TEM–EDS mapping to observe the distribution of elements in the samples. The chemical bonding states and crystal structures were examined X-ray photoelectron spectroscopy (XPS, ESCALAB 250) with an Al  $K\alpha$  X-ray source using X-ray diffractometry (XRD, Rigaku D/MAX2500 V) in the range from  $10^\circ$  to  $90^\circ$  with a step size of  $0.02^\circ$ . The binding energies of spectrum in XPS are standardized to the C 1s core level (284.5 eV). The surface properties such as the specific surface area, pore volume, average pore diameter, and pore volume fraction were performed by Brunauer-Emmett-Teller (BET) method using  $N_2$  adsorption/desorption.

#### 2.4. Electrochemical characterization

Electrochemical measurements were performed using coin cells (CR2032, Hohsen Corporation), which are consist of SCS as the anode, Li metal foil (Honjo Chemical, 99.8%) as the cathode, a 1.0 M  $LiPF_6$  solution in a mixture of ethylene carbonate–dimethyl carbonate (1:1) as the electrolyte, and a porous polypropylene membrane (Celgard 2400) as the separator. The SCS electrodes were prepared on a Cu foil substrate (Nippon Foil, 18  $\mu m$ ) as the current collector using coating an  $\gamma$ -methyl-2-pyrrolidinone solvent (NMP, Aldrich) based slurry with a mixture of 70 wt% of active materials, 20 wt% PVDF as the binder, and 10 wt% Ketjen black as the conducting material. The resultant electrodes were dried in an oven at  $100^\circ C$  for 12 h. All coin cells were assembled in a high-purity argon-filled glove box with  $H_2O$  and  $O_2$  contents less than 5 ppm. The discharge–charge tests carried out using a battery cycler system (WonATech Corp., WMPG 3000) in the potential range of 0.0–3.0 V (versus  $Li/Li^+$ ) at  $25^\circ C$  in an incubator. The cycling stability was observed up to 100 cycles at a current density of  $100\text{ mA g}^{-1}$ . The high-rate performance was measured at current densities of 100, 300, 500, 700, 1000, and 2000  $mA g^{-1}$ . The ultrafast performance was measured up to 100 cycles at current densities of  $2000\text{ mA g}^{-1}$ . EIS measurements were investigated in the frequency range of  $10^5$  to  $10^{-2}$  Hz by applying an AC signal of 5 mV. Cyclic voltammetry (CV) measurements were examined at a scan rate of  $0.1\text{ mV s}^{-1}$  in the voltage range of 0–3 V (versus  $Li/Li^+$ ) using a potentiostat/galvanostat (Eco chemie Autolab, PGSTAT302N). For comparison, a commercial Sn (Sigma-Aldrich) and a commercial graphite (MTI Korea) were purchased.

### 3. Results and discussion

Fig. 2 is a schematic illustration of an ideal synthetic route to the

unique SCS architecture. As shown in Fig. 2a, Sn cations are evenly distributed and impregnated in the porous spoilt tofu (Pulmuone Co., Ltd., Korea), which is an organic framework with micropores of molecular dimensions, and then dewatered. The impregnated tofu was dried at  $80^\circ C$  in air to remove water, as shown in Fig. 2b. Finally, carbonisation at  $800^\circ C$  for 2 h in a nitrogen atmosphere afforded a porous carbon framework, while the Sn cations were in situ converted to uniform well-dispersed ultrasmall Sn nanocrystals ( $<2\text{ nm}$ ). During the carbonisation in the nitrogen atmosphere,  $SnO_2$  was transformed to Sn via the reaction  $SnO_2 + N \rightarrow Sn + NO_2$ . In this study, the spoilt tofu-derived carbon framework with embedded ultrasmall Sn nanocrystals (Fig. 2c) obtained using 30 wt%  $SnCl_2 \cdot 2H_2O$  is referred to as SCS-30.

The chemical bonding states and crystal structures were examined using XPS with an Al  $K\alpha$  X-ray source and XRD in the range from  $10^\circ$  to  $90^\circ$  with a step size of  $0.02^\circ$ . The XPS binding energies were standardized to the C 1s core level (284.5 eV). SCS-30 derived from spoilt tofu was synthesised by simple impregnation and carbonisation. To investigate the chemical bonding states, XPS measurements were carried out, as shown in Fig. 3a. The Sn 3d XPS spectrum of SCS-30 showed two different signals at  $\sim 493.5$  and  $\sim 498.0$  eV with a spin energy separation of 8.5 eV, corresponding to  $3d_{3/2}$  and  $3d_{5/2}$  photoelectrons of metallic Sn, respectively [20,21]. These results indicate that nanocrystals are entirely composed of metallic Sn without any oxide states, such as SnO and  $SnO_2$ . In other words, the carbon framework blocks the oxide states and retains metallic Sn. The structure and morphology of the as-synthesised SCS were examined by SEM and TEM. Based on SEM imaging (Fig. 3b), the architecture size of SCS-30 with semi-block morphology is in the range of 0.7–1.5  $\mu m$ . SCS-30 showed a smooth surface (Fig. 3c) without any beads of agglomerated Sn, implying that the Sn nanocrystals were embedded within the porous carbon framework. These nanocrystals were of ultrasmall size (2.1–2.7 nm), as evidenced by TEM and high-resolution TEM (HRTEM) imaging (Fig. 3d and e). HRTEM images of SCS-30 show lattice fringes with a spacing of 0.29 nm, which corresponds to the (200) plane of Sn [22,23]. The unique architecture of ultrasmall Sn nanocrystals effectively provides a high contact area between Sn and electrolyte, leading to LIBs with high specific capacity. In addition, the porous carbon framework covered most of the Sn nanocrystals in SCS-30. To further investigate the uniform distribution of Sn and carbon atoms, EDS mapping of SCS-30 was performed, with the results shown in Fig. 3f. These results confirm that the C and Sn atoms were uniformly dispersed in the carbon framework. Moreover, the EDS findings confirm that Sn atoms are totally encapsulated by carbon atoms, which means that the

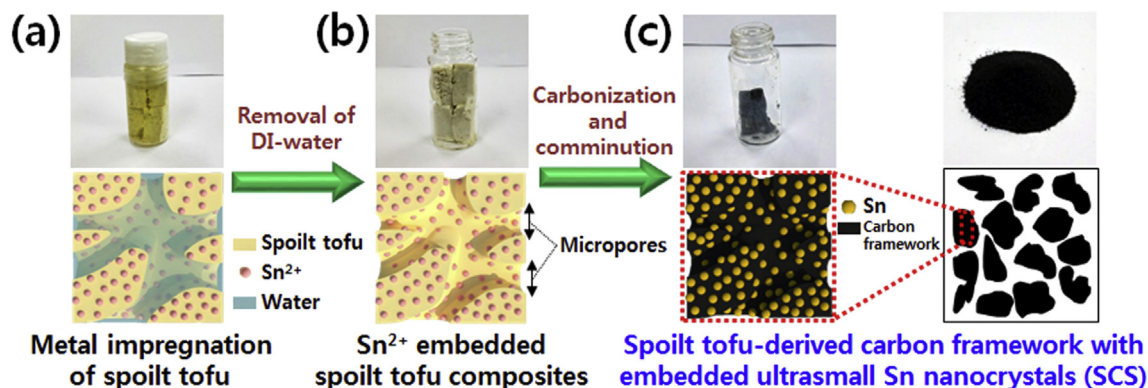
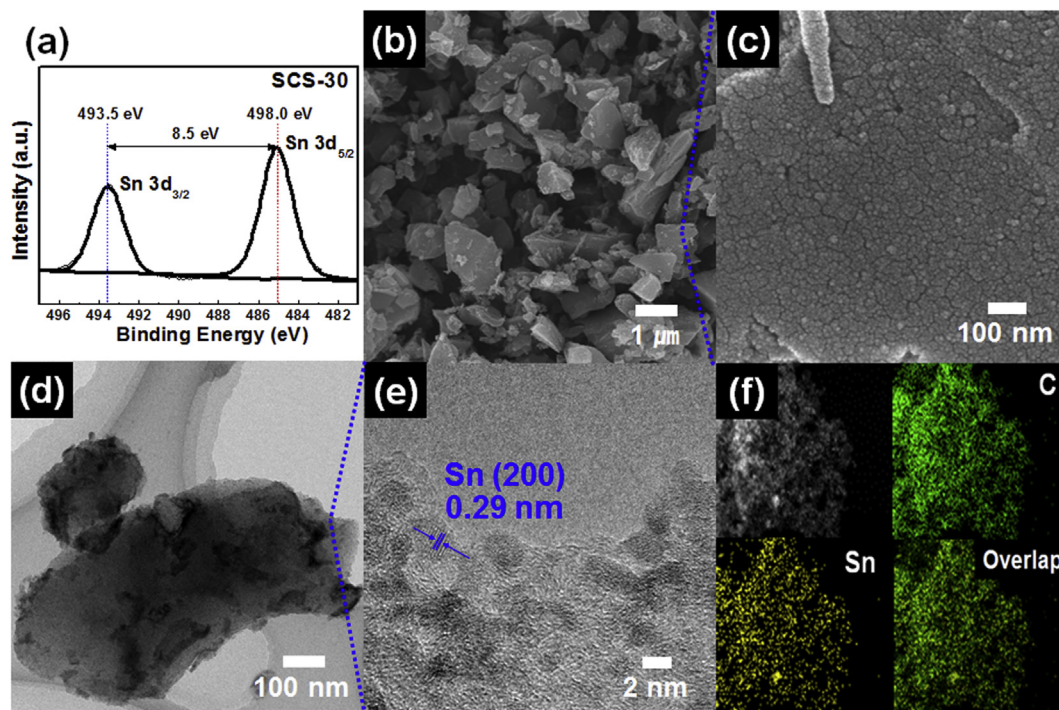


Fig. 2. Schematic illustration of an ideal synthetic route for the unique SCS architecture. (a) Metal impregnation of spoilt tofu. (b)  $Sn^{2+}$ -embedded spoilt tofu composites. (c) SCS obtained by carbonisation.



**Fig. 3.** Structural and morphological properties of SCS-30. (a) Sn 3d XPS spectra. (b) Low-resolution and (c) high-resolution FESEM images. (d) Low-resolution and (e) high-resolution TEM images. (f) TEM image and EDS mapping data.

wrapped Sn nanocrystals are in a porous carbon framework. Thus, the porous carbon framework can not only improve the dispersion of Sn nanocrystals but also firmly accommodate the aggregation of Sn nanocrystals from a volume expansion, leading to improved high-rate performance and enhanced cycling stability of LIBs [11,24].

To further verify the morphological structure of a carbon framework, SCS-20, and SCS-40, SEM and TEM analysis were carried out. Fig. 4 shows (a–c) low-resolution and (d–f) high-resolution FESEM images of a carbon framework, SCS-20, and SCS-40. The carbon framework (Fig. 4a and d) and SCS-20 (Fig. 4b and e) had a smooth surface. However, SCS-40 (Fig. 4c and f) had a

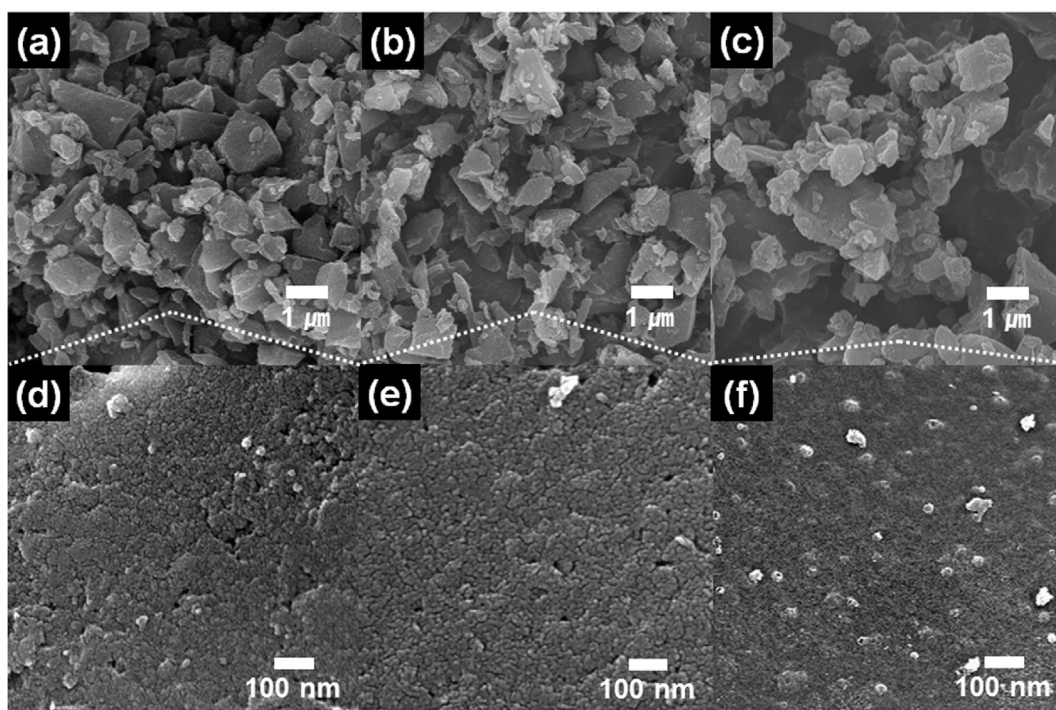


**Fig. 4.** (a–c) Low-resolution and (d–f) high-resolution FESEM images of a carbon framework, SCS-20, and SCS-40.

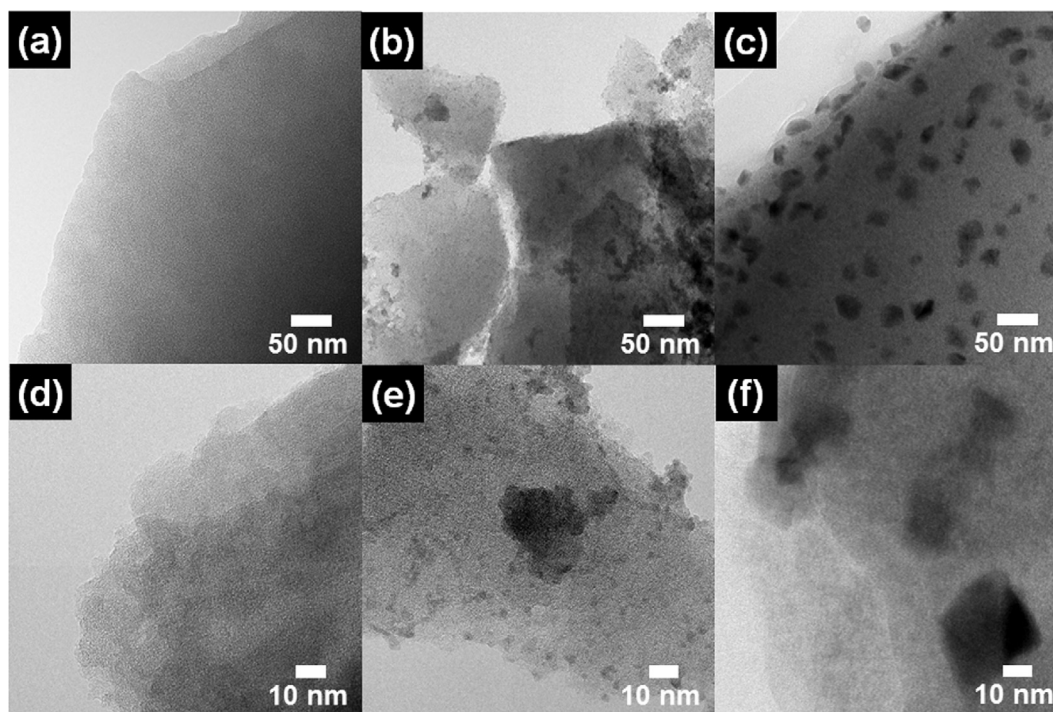


Fig. 5. (a–c) Low-resolution and (d–f) high-resolution TEM images of a carbon framework, SCS-20, and SCS-40.

rough surface, since Sn nanocrystals agglomerated mostly in the porous carbon framework.

Fig. 5 displays (a–c) low-resolution and (d–f) high-resolution TEM images of a carbon framework, SCS-20, and SCS-40. The carbon framework (Fig. 5a and d) presented a uniform contrast owing to only a single carbon phase. SCS-20 (Fig. 5b and e) was relatively dark, signifying the presence of Sn nanoparticles. The size of the Sn nanocrystals in SCS-40 was in the range of 21–31 nm (Fig. 5c and f). The formation of agglomerated Sn nanocrystals in SCS-40 is attributed to the large amount of Sn precursor in spoilt tofu. These characteristics would result in poor electrochemical LIB performance.

Fig. 6 shows XRD results of a carbon framework, SCS-20, SCS-30,

and SCS-40. The carbon framework exhibited the broad diffraction peak at  $25^\circ$ , corresponding to the (002) layers of graphite [12]. The main characteristic diffraction peaks of SCS-20, SCS-30, and SCS-40 were observed at  $30.6^\circ$ ,  $32.0^\circ$ ,  $43.9^\circ$ , and  $44.9^\circ$ , which correspond to the (200), (101), (220), and (211) planes of Sn, respectively (space group  $I4_1/amd$  [141]; JCPDS card No. 862264). These XRD results are in good agreement with the XPS and TEM results. In addition, as the Sn precursor was increased, the intensity of the diffraction peaks of the Sn phase become increasing because of the increased size of Sn nanocrystals, which is in good agreement with the FESEM and TEM results. In addition, the grain sizes of the Sn can be calculated by the diffraction patterns of SCS-30 using the Scherrer equation (which  $\lambda$  is the X-ray wavelength,  $\beta$  is the full width at half-maximum, and  $\theta$  is the Bragg angle)

$$D = 0.9\lambda/(\beta \cos \theta) \quad (1)$$

The size of Sn for SCS-30 is calculated to be 2.5 nm, based on the (200) and (101) planes.

To further estimate the properties of the porous carbon framework, such as specific surface area, pore volume, and average pore diameter, BET analysis was performed using  $N_2$  adsorption/desorption, as shown in Fig. S1. The isotherms of the porous carbon framework in SCS-20, SCS-30, and SCS-40 exhibiting a steep increase at low relative pressures ( $P/P_0 < 0.1$ ) show typical Type-I behaviour, based on the IUPAC nomenclature, i.e., these samples contain a large amount of micropores (width  $< 2$  nm) [6–8]. Consequently, SCS-30 provides a high specific surface area of  $307 \text{ m}^2 \text{ g}^{-1}$  due to the porous carbon framework. As the Sn nanocrystal loading was increased, the specific surface area decreased due to the presence of Sn nanocrystals in the porous carbon framework, which is in good agreement with the TEM results. Detailed information on the sample specific surface area, total pore volume, and average pore diameter is summarised in Table S1. During the discharge-charge process in LIBs, the porous carbon framework with high surface area can efficiently allow the

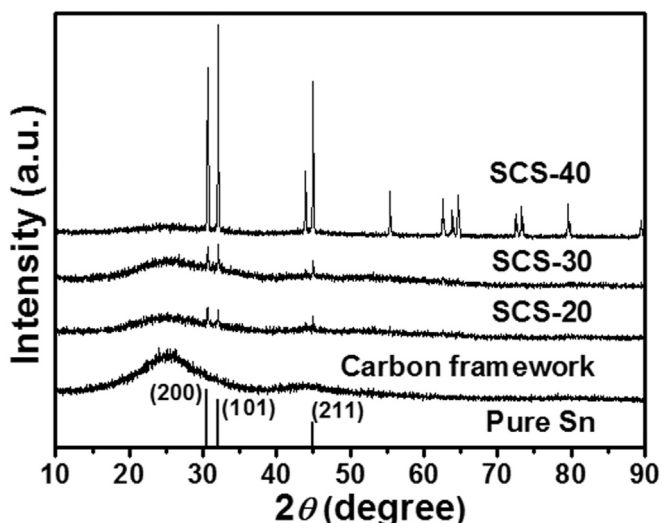


Fig. 6. XRD patterns of a carbon framework, SCS-20, SCS-30, and SCS-40.

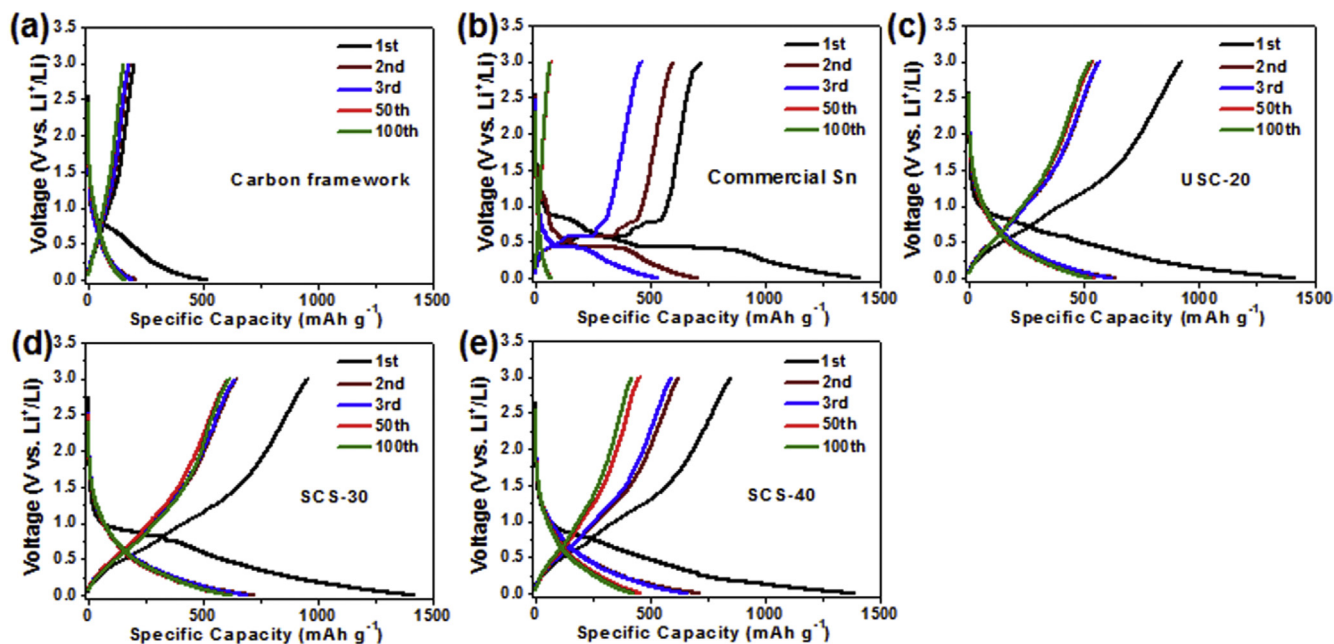


Fig. 7. Charge–discharge curves of (a) a carbon framework, (b) a commercial Sn, (c) SCS-20, (d) SCS-30, and (e) SCS-40 at a current density of  $100 \text{ mA g}^{-1}$  in the potential range of 0.0–3.0 V for 1st, 2nd, 3rd, 50th and 100th cycles.

favourable Li-ion diffusion, leading to improved high-rate performance [11,24]. The analysis results demonstrate that SCS-30 encompasses three main advantages of a porous carbon framework as well as the good distribution of ultrasmall Sn nanocrystals.

Electrochemical analysis was performed using coin-type cells featuring SCS as the anode, Li metal foil as the cathode, a 1.0 M LiPF<sub>6</sub> solution in a mixture of ethylene carbonate and dimethyl carbonate (1:1) as the electrolyte, and a porous polypropylene membrane as the separator. For comparison, the porous carbon framework was prepared without SnCl<sub>2</sub>·2H<sub>2</sub>O. In addition, commercial Sn metal (<150 nm particle size) was purchased from Sigma-Aldrich (no. 576883) for comparison.

Charge–discharge curves of a carbon framework, a commercial Sn, SCS-20, SCS-30, and SCS-40 at a current density of  $100 \text{ mA g}^{-1}$  in the potential range of 0.0–3.0 V for 1st, 2nd, 3rd, 50th and 100th cycles are shown in Fig. 7a–e, respectively. The carbon framework electrode (Fig. 7a) indicated an inclined curve without the formation of a voltage plateau during the first discharge process, which means the typical discharge property of carbon-based materials [11,12]. The voltage profiles of a commercial Sn, SCS-20, SCS-30, and SCS-40 electrodes (Fig. 7b–e) indicated the typical characteristics of Sn electrode. These electrodes exhibited long slope starting from around 1.0 V–0.0 V, which can be attributed to the electrochemical reactions of Sn with Li to form Li<sub>x</sub>Sn alloys and intercalation of lithium into carbon reactions (Li<sub>x</sub>C) [16]. In addition, the SCS-20, SCS-30, and SCS-40 electrodes showed the more gradual sloping curves, indicating that Sn nanocrystals can provide the rapid electrochemical reaction during the cycling [12]. The first specific discharge and charge capacities were 1413 and 921  $\text{mA h g}^{-1}$  for SCS-20, 1417 and 956  $\text{mA h g}^{-1}$  for SCS-30, and 1411 and 864  $\text{mA h g}^{-1}$  for SCS-40 electrodes, respectively, being much higher than the values for the commercial Sn electrode (1410 and 719  $\text{mA h g}^{-1}$ ) and the porous carbon framework electrode (512 and 201  $\text{mA h g}^{-1}$ ). The first discharge capacities of all electrodes were higher than the theoretical value due to the direct formation of solid-electrolyte interface (SEI) layers that can store charge via interfacial charging at the metal/Li<sub>2</sub>O interface [11,25]. The SEI

layers are usually formed during the first cycle owing to the reductive decomposition of electrolyte components on the electrode surface, leading to high initial irreversible capacity losses [11,25,26]. Nonetheless, the SCS-30 electrode showed a higher coulombic efficiency (67.5%) than the commercial Sn electrode (51%), the porous carbon framework electrode (39.3%), the SCS-20 electrode (65.2%), and the SCS-40 electrode (61.3%). This suggests that the well-dispersed Sn nanocrystals embedded in the porous carbon framework can largely prevent injurious electrochemical reactions of Sn with the electrolyte.<sup>21</sup> In addition, all SCS electrodes reached a coulombic efficiency of almost 100% after five cycles, implying high reversibility.

Fig. 8a shows the cycling performance of commercial Sn, porous carbon framework, SCS-20, SCS-30, and SCS-40 electrodes at a current density of  $100 \text{ mA g}^{-1}$  up to 100 cycles in the potential range of 0.0–3.0 V (vs. Li/Li<sup>+</sup>). The commercial Sn electrode exhibited a rapid specific capacity drop to 72  $\text{mA h g}^{-1}$  after 100 cycles, indicating large volume expansion due to Li-ion insertion/extraction during cycling. Thus, Sn metal is necessarily required to form a composite with carbon. To solve these problems, we first prepared the novel porous carbon framework derived from spoilt tofu. The corresponding electrode showed a specific capacity (162  $\text{mA h g}^{-1}$  after 100 cycles) similar to that of the commercial graphite electrode (196  $\text{mA h g}^{-1}$ ), as shown in Fig. S2. These results confirmed the successful synthesis of a porous carbon framework for use in LIBs. Remarkably, the SCS-30 electrode displayed notable cycling stability with a specific capacity of 621  $\text{mA h g}^{-1}$  after 100 cycles, which is nearly 8.6 times higher than that of the commercial Sn electrode. This performance is also superior to those of Sn-based carbon anode materials reported previously, as summarised in Table S2 [27–36]. However, the SCS-20 electrode showed a relatively low specific discharge capacity of 533  $\text{mA h g}^{-1}$  after 100 cycles compared to SCS-30 due to the small amount of Sn nanocrystals in the carbon framework (Fig. 5e). Therefore, we believe that the excellent cycling stability of SCS-30 is mainly ascribed to two factors. First, the porous carbon framework derived from spoilt tofu could efficiently deal with the volume expansion of Sn

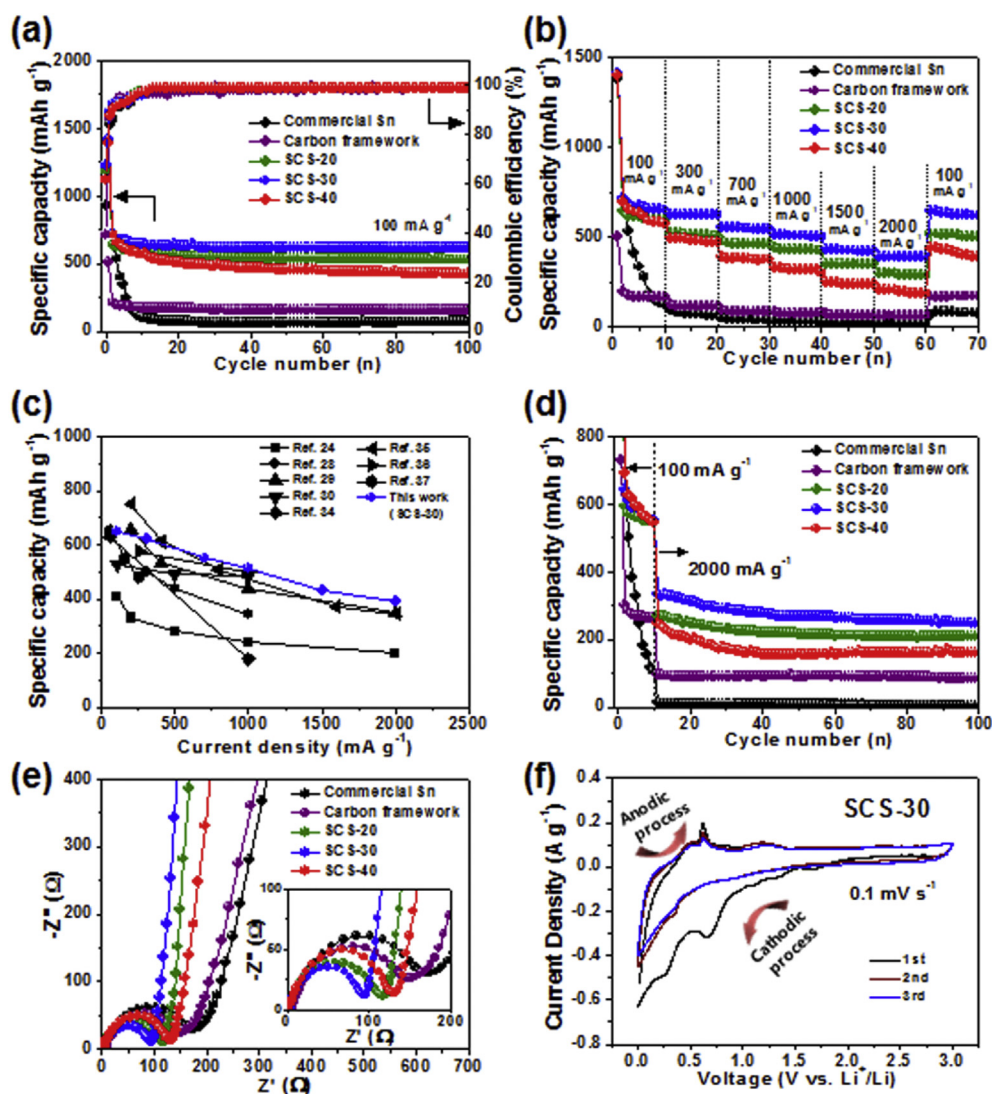


**Fig. 8.** Electrochemical characteristics of SCS electrodes. (a) The cycling stability of charge–discharge capacities of a commercial Sn, carbon framework, SCS-20, SCS-30, and SCS-40 at current densities of 100 mA g<sup>-1</sup> up to 100 cycles. (b) The high-rate performance at current densities of 100, 300, 700, 1000, 1500, 2000, and 100 mA g<sup>-1</sup>. (c) Comparison of high-rate performance with previously reported studies of Sn and carbon composite-based anode materials in LIBs. (d) The high-rate performance of a commercial Sn, a carbon framework, SCS-20, SCS-30, and SCS-40 at current density of 2000 mA g<sup>-1</sup> up to 100 cycles. (e) Nyquist plots in the frequency range of 10<sup>5</sup> to 10<sup>-2</sup> Hz at an open-circuit potential. (f) CV curves of SCS-30 in the potential range of 0.0–3.0 V (versus Li/Li<sup>+</sup>) at a scan rate of 0.1 mV s<sup>-1</sup>.

nanoparticles during Li-ion insertion/extraction processes. Second, the good dispersion of ultrasmall Sn nanocrystals could significantly increase the number of electroactive sites, owing to the high number of contacts between Sn and Li ions. In addition, due to the large size of agglomerated Sn nanocrystals, the SCS-40 electrode exhibited relatively low cycling stability with a specific discharge capacity of 421 mA h g<sup>-1</sup> after 100 cycles.

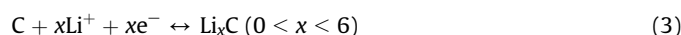
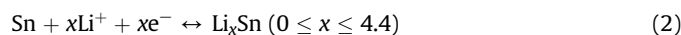
It should be further noted that the high-rate performance is an important issue to consider in designing high-performance LIBs. Fig. 8b displays the high-rate performance of all electrodes obtained at current densities of 100, 300, 700, 1000, 1500, 2000, and 100 mA g<sup>-1</sup>. Notably, the SCS-30 electrode showed an outstanding high-rate performance of 649 to 385 mA h g<sup>-1</sup> as the current densities were increased from 100 to 2000 mA g<sup>-1</sup>, respectively, subsequently recovering to 645 mA h g<sup>-1</sup> (99% of the original specific capacity) when the current density returned to 100 mA g<sup>-1</sup>. Remarkably, the outstanding high-rate performance of SCS-30 is one of the highest values when compared to the previously reported results for Sn-based carbon anode materials (Fig. 8c)

[29–31,36–40]. Furthermore, the SCS-30 electrode showed a high specific capacity of 250 mA h g<sup>-1</sup> after 100 cycles at a high current density of 2000 mA g<sup>-1</sup> (Fig. 8d), meaning that the optimised SCS electrode can be efficiently used in LIB applications where ultrafast discharge-charge is required. The outstanding high-rate performance of the SCS-30 electrode can mainly be attributed to the shorter diffusion pathway for both ions and electrons due to the high porosity of the carbon framework as well as to the well-dispersed ultrasmall Sn nanocrystals.

To further understand the reasons for the better high-rate performance of the SCS-30 electrode, EIS measurements were performed using fresh cells. Fig. 8e shows the Nyquist plots of all electrodes in the frequency range of 10<sup>5</sup> to 10<sup>-2</sup> Hz at an open-circuit potential. The semicircle in the high-frequency region is ascribed to the charge transfer resistance ( $R_{ct}$ ) at the anode-electrolyte interface, and the straight line in the low-frequency range, referred to as the Warburg impedance, corresponds to Li-ion diffusion in the anode [11,16]. SCS-30 shows the lowest  $R_{ct}$  and low Warburg impedance compared to the other electrodes,

indicating improved charge transfer kinetics and a shorter Li-ion diffusion pathway. These results are in good agreement with those of the high-rate performance. Thus, the EIS results of SCS-30 with ultrasmall Sn nanocrystals suggest that the improved charge transfer kinetics is attributed to the large number of active sites due to the increased number of charge transfer channels compared to SCS-20 and SCS-40 electrodes.

To further understand the electrochemical properties of the SCS-30 electrode, CV measurements were performed using a potentiostat/galvanostat in the potential range of 0–3 V (vs. Li/Li<sup>+</sup>) at a scan rate of 0.1 mV s<sup>-1</sup>. The CV curve clearly shows the reduction (Li insertion) and oxidation peaks (Li extraction), as shown in Fig. 8f, which is a typical feature of Sn [27,30,32,35,38,40]. In the first cathodic scan, the broad reduction peaks between 0.3 and 0.8 V are related to the electrochemical reactions between Sn and Li to form Li<sub>x</sub>Sn alloys, while the peak at 0 V is related to the intercalation of Li into the porous carbon framework, forming Li<sub>x</sub>C. The oxidation peak between 0.4 and 0.8 V in the first anodic scan corresponds to the de-alloying of Li<sub>x</sub>Sn. It can be seen that the curves of the second and third scans are almost superimposed, indicating the excellent electrochemical reversibility of Li storage in the SCS-30 electrode. However, no broad reduction peaks in the second and third cathodic scans were attributed to the occurrence of irreversible processes, e.g., the formation of an SEI layer. Therefore, the electrochemical alloying reaction of SCS-30 includes the following steps [29,33,40]:



Thus, we have achieved exceptional lithium storage performance using our newly designed architecture, which can be explained by its several advantages. The porous carbon framework derived from spoiled tofu can effectively deal with the volume expansion of Sn nanocrystals during cycling, leading to improved cycling stability as well as enhanced high-rate performance. In addition, the well-dispersed ultrasmall Sn nanocrystals can provide remarkably improved specific capacity owing to the high number of contact sites between Sn and Li ions and an enhanced high-rate performance due to shorter diffusion pathway for Li ions. Thus, SCS derived from spoiled tofu has excellent potential as a novel anode for high-performance LIBs.

#### 4. Conclusions

SCS derived from spoiled tofu was successfully synthesised by simple impregnation and carbonisation using spoiled tofu and a Sn precursor. The optimised SCS-30 exhibited unique architecture featuring a porous carbon framework embedded with ultrasmall Sn nanocrystals (2.1–2.7 nm). The optimised SCS-30 electrode showed improved lithium storage properties, including the highest coulombic efficiency of 67.5%, outstanding cycling stability (621 mA h g<sup>-1</sup> after 100 cycles), and excellent high-rate performance (250 mA h g<sup>-1</sup> at 2000 mA g<sup>-1</sup>) compared to the SCS-20 and SCS-40 electrodes and the commercial Sn electrode. This outstanding electrochemical performance can be explained by the following combined effects: (I) the outstanding cycling stability is related to the porous carbon framework, which prevents the severe volume-expansion stress of Sn; and (II) its improved specific capacity and high-rate performance is related to the good dispersion of ultrasmall Sn nanocrystals providing numerous active sites and a shorter diffusion pathway for Li ions. Thus, the facile approach using spoiled tofu also provides promising materials for the synthesis of carbon frameworks and high-performance LIBs. Moreover, this

novel approach using food waste is an attractive strategy for other high-performance applications such as energy storage devices, electrocatalysts, and sensors.

#### Acknowledgments

This research was supported by Basic Science Research Program through the National Research Foundation of Korea (NRF) funded by the Ministry of Science, ICT and Future Planning (NRF-2015R1A1A1A05001252).

#### Appendix A. Supplementary data

Supplementary data related to this article can be found at <http://dx.doi.org/10.1016/j.jallcom.2017.06.067>.

#### References

- [1] C.S. Lin, L.A. Pfaltzgraff, L.H. Davila, E.B. Mofufo, S. Abderrahim, J.H. Clark, A.A. Koutinas, N. Kopsahelis, K. Stamatelidou, F. Dickson, S. Thankappan, Z. Mohamed, R. Brocklesby, R. Luque, Food waste as a valuable resource for the production of chemicals, materials and fuels. Current situation and global perspective, *Energy Environ. Sci.* 6 (2013) 426–464.
- [2] I.V. Gursel, T. Noel, Q. Wang, V. Hessel, Separation/recycling methods for homogeneous transition metal catalysts in continuous flow, *Green Chem.* 17 (2015) 2012–2026.
- [3] US Environmental Protection Agency America's Food Waste Problem, 2016.
- [4] Q. Zhu, F. Wu, M. Saito, E. Tatsumi, L. Yin, Effect of magnesium salt concentration in water-in-oil emulsions on the physical properties and microstructure of tofu, *Food Chem.* 201 (2016) 197–204.
- [5] F. Rossi, G.E. Felis, A. Martinelli, B. Calcavecchia, S. Torriani, Microbiological characteristics of fresh tofu produced in small industrial scale and identification of specific spoiling microorganisms (SSO), *LWT-Food Sci. Technol.* 70 (2016) 280–285.
- [6] X. Lu, F. Yang, Y. Wang, X. Geng, P. Xiao, The influence of graphene/carbon mass ratio on microstructure and electrochemical behavior in the graphene–SnO<sub>2</sub>–carbon composite as anodes for Li-ion batteries, *J. Alloys Compd.* 635 (2015) 202–210.
- [7] Y.-W. Lee, G.-H. An, B.-S. Kim, J. Hong, S. Park, E.-H. Lee, Y. Cho, J. Lee, P. Giraud, S.N. Cha, H.-J. Ahn, J.I. Sohn, J.M. Kim, Synergistic effects of a multifunctional graphene based interlayer on electrochemical behavior and structural stability, *ACS Appl. Mat. Interfaces* 8 (2016) 17651–17658.
- [8] D. Zhou, W.-L. Song, X. Li, L.-Z. Fan, Y. Dong, Tin nanoparticles embedded in porous N-doped graphene-like carbon network as high-performance anode material for lithium-ion batteries, *J. Alloys Compd.* 699 (2017) 730–737.
- [9] J.-Y. Lin, M.-H. Chou, Y.-C. Kuo, Rapid synthesis of tin oxide decorated carbon nanotube nanocomposites as anode materials for lithium-ion batteries, *J. Alloys Compd.* 589 (2014) 472–478.
- [10] M. Uysal, T. Cetinkaya, A. Alp, H. Akbulut, Active and inactive buffering effect on the electrochemical behavior of Sn–Ni/MWCNT composite anodes prepared by pulse electrodeposition for lithium-ion batteries, *J. Alloys Compd.* 645 (2015) 235–242.
- [11] G.-H. An, J.I. Sohn, H.-J. Ahn, Hierarchical encapsulated architecture of hybrid carbon-hollow manganese oxide nanotubes with a porous-wall structure for high-performance electrochemical energy storage, *J. Mat. Chem. A* 4 (2016) 2049–2054.
- [12] G.-H. An, D.-Y. Lee, Y.-J. Lee, H.-J. Ahn, Ultrafast lithium storage using antimony-doped tin oxide nanoparticles sandwiched between carbon nanofibers and a carbon skin, *ACS Appl. Mat. Interfaces* 8 (2016) 30264–30270.
- [13] M. Cao, M. Zhang, L. Xing, Q. Wang, X.-Y. Xue, One-step preparation of pomegranate-shaped Sn/SnO<sub>x</sub>/nanocarbon composites for fabricating ultrafast-charging/long-life lithium-ion battery, *J. Alloys Compd.* 694 (2017) 30–39.
- [14] H. Liu, R. Hu, C. Huang, W. Sun, H. Zhang, M. Zhu, Toward cyclic durable core/shell nanostructure of Sn–C composite anodes for stable lithium storage by simulating its lithiation-induced internal strain, *J. Alloys Compd.* 704 (2017) 348–358.
- [15] R. Liu, W. Su, P. He, C. Shen, C. Zhang, F. Su, C.-A. Wang, Synthesis of SnO<sub>2</sub>/Sn hybrid hollow spheres as high performance anode materials for lithium ion battery, *J. Alloys Compd.* 688 (2016) 908–913.
- [16] G.-H. An, H.-J. Ahn, Carbon nanofiber/cobalt oxide nanopyramid core-shell nanowires for high-performance lithium-ion batteries, *J. Power Sourc.* 272 (2014) 828–836.
- [17] S. Sengupta, A. Patra, M. Akhtar, K. Das, S.B. Majumder, S. Das, 3D microporous Sn–Sb–Ni alloy impregnated Ni foam as high-performance negative electrode for lithium-ion batteries, *J. Alloys Compd.* 705 (2017) 290–300.
- [18] X. Li, X. Li, L. Fan, Z. Yu, B. Yan, D. Xiong, X. Song, S. Li, K.R. Adair, D. Li, X. Sund, Rational design of Sn/SnO<sub>2</sub>/porous carbon nanocomposites as anode materials for sodium-ion batteries, *Appl. Surf. Sci.* 412 (2017) 170–176.

- [19] H. Wang, X. Du, X. Jiang, Y. Chai, X. Yang, R. Yuan, Pomegranate-like porous carbon coated  $\text{Cu}_x\text{Sn}_y/\text{Sn}/\text{SnO}_2$  submicrospheres as superior lithium ion battery anode, *Chem. Eng. J.* 313 (2017) 535–543.
- [20] C.D. Gu, Y.J. Mai, J.P. Zhou, Y.H. You, J.P. Tu, Non-aqueous electrodeposition of porous tin-based film as an anode for lithium-ion battery, *J. Power Sourc.* 214 (2012) 200–207.
- [21] H. Ma, K. Teng, Y. Fu, Y. Song, Y. Wang, X. Dong, Synthesis of visible-light responsive  $\text{Sn-SnO}_2/\text{C}$  photocatalyst by simple carbothermal reduction, *Energy Environ. Sci.* 4 (2011) 3067–3074.
- [22] Q.-C. Pan, Y.-G. Huang, H.-Q. Wang, G.-H. Yang, L.-C. Wang, J. Chen, Y.-H. Zan, Q.-Y. Li,  $\text{MoS}_2/\text{C}$  nanosheets encapsulated  $\text{Sn}$  nanoparticles as high-performance lithium-ion battery anode material, *Electrochim. Acta* 197 (2016) 50–57.  $\text{Sn@SnO}$ .
- [23] Y.-G. Huang, Q.-C. Pan, H.-Q. Wang, Z.-X. Yan, G.-H. Yang, Y.-H. Chen, Q. Wu, Q.-Y. Li,  $\text{Sn}/\text{SnO}_x$  embedded in carbon nanosheets as high-performance anode material for lithium ion battery, *Ceram. Int.* 42 (2016) 4586–4593.
- [24] Z. Zhu, S. Wang, J. Du, Q. Jin, T. Zhang, F. Cheng, J. Chen, Ultrasmall Sn nanoparticles embedded in nitrogen-doped porous carbon as high-performance anode for lithium-ion batteries, *Nano Lett.* 14 (2014) 153–157.
- [25] A. Abouimrane, Y. Cui, Z. Chen, I. Belharouak, H.B. Yahia, H. Wu, R. Assary, L.A. Curtiss, K. Amine, Enabling high energy density Li-ion batteries through  $\text{Li}_2\text{O}$  activation, *Nano Energy* 27 (2016) 196–201.
- [26] G. Huang, X. Guo, X. Cao, Q. Tian, H. Sun, 3D network single-phase  $\text{Ni}_{0.9}\text{Zn}_{0.1}\text{O}$  as anode materials for lithium-ion batteries, *Nano Energy* 28 (2016) 338–345.
- [27] D. Deng, J.Y. Lee, Reversible storage of lithium in a rambutan-like tin–carbon electrode, *Angew. Chem. Int. Ed.* 48 (2009) 1660–1663.
- [28] M. Alaf, D. Gultekin, H. Akbulut, Electrochemical properties of free-standing  $\text{Sn}/\text{SnO}_2$ /multi-walled carbon nano tube anode papers for Li-ion batteries, *Appl. Surf. Sci.* 275 (2013) 244–251.
- [29] J. Zhang, Z. Ma, W. Jiang, Y. Zou, Y. Wang, C. Lu, Sandwich-like  $\text{CNTs@SnO}_2/\text{SnO}/\text{Sn}$  anodes on three-dimensional Ni foam substrate for lithium ion batteries, *J. Electroanal. Chem.* 767 (2016) 49–55.
- [30] K.-C. Hsu, C.-E. Liu, P.-C. Chen, C.-Y. Lee, H.-T. Chiu, One-step vapor-solid reaction growth of  $\text{Sn@C}$  core-shell nanowires as an anode material for Li-ion batteries, *J. Mat. Chem.* 22 (2012) 21533–21539.
- [31] G. Wang, Y.Q. Ma, Z.Y. Liu, J.N. Wu, Novel highly porous Sn–C composite as high performance anode material for lithium-ion batteries, *Electrochim. Acta* 65 (2012) 275–279.
- [32] C. Cui, X. Liu, N. Wu, Y. Sun, Facile synthesis of core/shell-structured Sn/ion-like carbon nanocapsules as high-performance anode material for lithium-ion batteries, *Mat. Lett.* 143 (2015) 35–37.
- [33] Y. Hu, Q.-R. Yang, J. Ma, S.-L. Chou, M. Zhu, Y. Li,  $\text{Sn}/\text{SnO}_2/\text{C}$  composite nanofibers as advanced anode for lithium-ion batteries, *Electrochim. Acta* 186 (2015) 271–276.
- [34] B. Luo, B. Wang, M. Liang, J. Ning, X. Li, L. Zhi, Reduced graphene oxide-mediated growth of uniform tin-core/carbon-sheath coaxial nanocables with enhanced lithium ion storage properties, *Adv. Mater.* 24 (2012) 1405–1409.
- [35] Z. Li, W. Lv, C. Zhang, J. Qin, W. Wei, J.-J. Shao, D.-W. Wang, B. Li, F. Kang, Q.-H. Yang, Nanospace-confined formation of flattened Sn sheets in pre-seeded graphenes for lithium ion batteries, *Nanoscale* 6 (2014) 9554–9558.
- [36] Q. Tian, Z. Zhang, L. Yang, S.-I. Hirano, Synthesis of  $\text{SnO}_2/\text{Sn@carbon}$  nanospheres dispersed in the interspaces of a three-dimensional  $\text{SnO}_2/\text{Sn@carbon}$  nanowires network, and their application as an anode material for lithium-ion batteries, *J. Mat. Chem. A* 2 (2014) 12881–12887.
- [37] P. Lian, J. Wang, D. Cai, G. Liu, Y. Wang, H.J. Wang, Design and synthesis of porous nano-sized  $\text{Sn@C}/\text{graphene}$  electrode material with 3D carbon network for high-performance lithium-ion batteries, *J. Alloys Compd.* 604 (2014) 188–195.
- [38] X. Bai, B. Wang, H. Wang, J. Jiang, Preparation and electrochemical properties of profiled carbon fiber-supported Sn anodes for lithium-ion batteries, *J. Alloys Compd.* 628 (2015) 407–412.
- [39] L. Ji, Z. Tan, T. Kuykendall, E.J. An, Y. Fu, V. Battaglia, Y. Zhang, Multilayer nanoassembly of Sn-nanopillar arrays sandwiched between graphene layers for high-capacity lithium storage, *Energy Environ. Sci.* 4 (2011) 3611–3616.
- [40] Y. Yu, L. Gu, G. Wang, A. Dhanabalan, P.A.V. Aken, J. Maier, Encapsulation of  $\text{Sn@carbon}$  nanoparticles in bamboo-like hollow carbon nanofibers as an anode material in lithium-based batteries, *Angew. Chem. Int. Ed.* 48 (2009) 6485–6489.